Limit analysis of bearing capacity for a circular footing subjected to eccentric loads

L'analyse limite de capacité portante des fondations circulaires sous chargement excentrique

H. Sekiguchi & S. Kobayashi – *Department of Civil Engineering, Kyoto University, Japan*

ABSTRACT: In this paper, limit analysis is applied to a bearing capacity problem of a circular rigid footing on a weightless Tresca material subjected to eccentric vertical loading. The upper-bound and lower-bound solutions obtained here reveal the range in which the exact solution exists. These theoretical results compare favorably with what has been obtained from bearing capacity tests on undrained cohesive soil. This kind of limit analysis has potential applications in the design of shallow foundations subjected to severe loading conditions.

RÉSUMÉ: Dans cet article, l'analyse limite est appliquée au problème de capacité portante d'une fondation rigide circulaire sur un matériau de Tresca de masse nulle soumis à un chargement vertical excentrique. Les solutions des frontières supérieures et inférieures obtenues révèlent les limites pour lesquelles une solution exacte existe. Ces résultats théoriques sont comparables aux expériences de capacité portante réalisées sur des sols cohésifs non secs. Cette sorte d'analyse limite possède des applications potentielles dans l'étude des fondations soumises à des conditions de chargement sévères.

1 INTRODUCTION

It is important to understand the bearing capacity of foundations under combined loads when designing offshore structures that are subjected to severe loading conditions, such as wave forces. The bearing capacity characteristics of rigid shallow foundations subjected to combined loading may be schematically illustrated in Fig. 1. The bearing capacity surface in load space has been derived on the basis of recent experimental results (e.g. Nova & Montrasio 1991, Dean et al. 1993, Houlsby & Martin 1993, Butterfield & Gottardi 1994). Note that this load space has three base vectors; vertical load V, horizontal load H and moment load M/B, where B is the width of a given footing. The maximum capacity under vertical centered loading is expressed as V_m. Parameters μ and ψ govern the shape of the bearing surface. Specifically, μ and ψ are gradients of the sectional curves cut by the plane $M/B = 0$ or $H = 0$, at the origin of the load space. The sectional curve of this bearing surface cut by the plane $H = 0$ or $V \sim M/B$ represents the bearing capacity under eccentric vertical loading.

Conventionally, the effective width concept for strip footings (Meyerhof 1953) along with the 'effective-and-equivalent' area concept for circular footings (Hansen 1961) are well known as methods for evaluating the bearing capacity under eccentric vertical loading. Although these methods have been extensively used in engineering practice, their theoretical nature has received little attention from the standpoint of plasticity theory.

This paper deals with a bearing capacity problem for a circular footing on Tresca ground subjected to eccentric vertical loads, for which an exact solution has not yet been obtained. Both the upper- and lower-bound solutions for this problem will be derived below in terms of limit analysis.

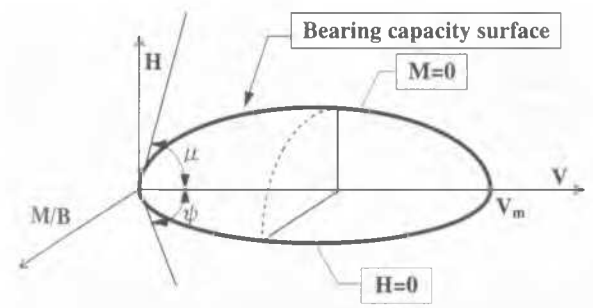

Figure 1: Bearing capacity surface in load space (schematic)

2 BEARING CAPACITY OF A CIRCULAR FOOTING SUBJECTED TO ECCENTRIC VERTICAL LOADING

Let us consider a bearing capacity problem in which a circular rigid footing with a radius a is subjected to eccentric vertical loading. The footing has a rough base and rests on a weightless Tresca material with a shear strength k. The vertical load acts on the point O' with an eccentricity e from the footing center O.

2.1 *Lower bound solution incorporating effective area concept*

This analysis offers a new look at the concept of an effectively loaded area. The most important consideration is that the effectively loaded area for a given eccentricity e should be sought in such a way that the stress field below the effective area is statically admissible. The effective area introduced here is illustrated in Fig. 2. In fact, one can think of a circular effective area just below the actual footing such that the reduced circular area is centered directly beneath the actual loading point, and that its radius $(a - e)$ is large enough to extend to the nearest edge of the actual footing. The vertical contact pressure σ_z over the remaining crescent-shaped area should be zero.

The stress field below the effective area may be constructed to be statically admissible, with reference to the Eason-Shield stress field (Eason & Shield 1960) which was originally proposed for a rigid rough plate on a Tresca material subjected to vertical centered loading. Cross section through the center of the footing O as well as the loading point is shown in Fig. 3. A statically admissible stress field beneath and around the footing (cf. area $O'ADEF$) was obtained by the method of stress characteristics. The plastic stress field can be extended to outer rigid regions without violating the yield criteria; that is to say, the yield function $f < 0$ in rigid regions. Thus, the stress field shown in Fig. 3 can be recognized as a statically admissible stress field in the entire domain. Note in this regard that line $AO'C$ represents the diameter of the effectively loaded circle. Since the effective circle is centered at point O' precisely below the actual lading point, its radius is equal to $(a - e)$. The stress field below the effective area is statically admissible and is axi-symmetric about the vertical line that passes through point O'.

The vertical load V which acts on the upper surface of the footing should be in equilibrium with the admissible stress field described above. The vertical contact pressures over the effective circle are not uniform in this case and take a particular axi-symmetrical distribution. In fact, its spatial average over the effective circle is equal to $6.05k$. It thus follows that

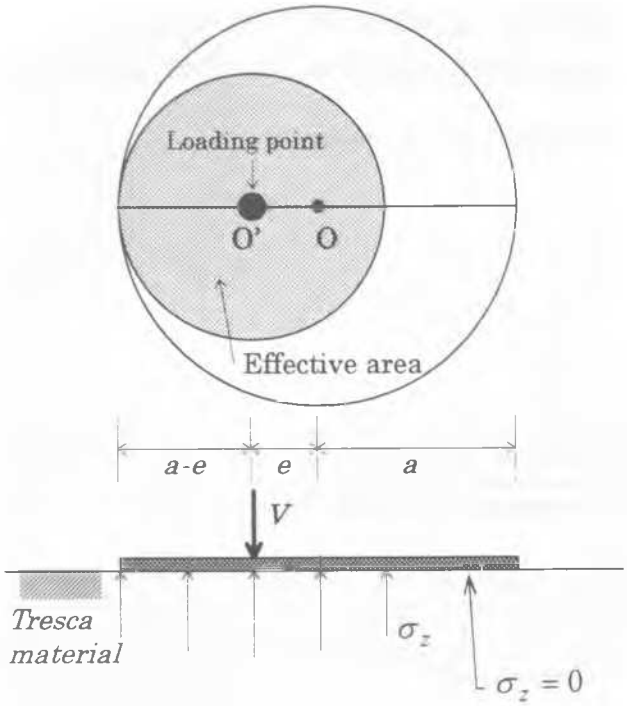

Figure 2: Effective area introduced for a circular rigid footing

$$V = 6.05k \cdot A_e, \quad M = V \cdot e \tag{1}$$

where $A_e = \pi(a-e)^2$. Elimination of eccentricity e from Eqs. (1) yields

$$\frac{M}{a \cdot V_m} = \frac{V}{V_m}\left(1 - \sqrt{\frac{V}{V_m}}\right) \tag{2a}$$

$$V_m = 6.05k \cdot A \tag{2b}$$

where A is the cross-sectional area of the circular footing which is equal to πa^2, and V_m represents the limiting bearing capacity for vertical centered loading.

The lower bound solution in the form of Eq. (2) is illustrated in Fig. 5 with a thick solid line. It will suffice here to mention that this limiting line approximates to a parabola in the plane $V/(kA)$ versus $M/(akA)$.

2.2 *Upper bound solution in terms of rotational failure mechanism*

Suppose that the ground below a rigid circular footing undergoes rotational failure by the action of an eccentric vertical load (Fig. 4). We refer to a Cartesian coordinate system (x, y, z) whose origin is taken at point A. The x-axis is taken along a horizontal axis of rotation (chain-dotted). Note that the circular footing rests on a plane $z = z_0$ and is centered at point O with $x = 0$ and $y = c$. The periphery of the footing is thus expressed as $x^2 + (y-c)^2 = a^2$, where a denotes the radius of the footing.

Based on this mechanism, the upper bound solution is evaluated by setting that the rate of the total internal dissipation energy along a failure surface $\dot{W}_{int}$ is equal to the rate of the total external work due to an eccentric vertical load $\dot{W}_{ext}$. The results obtained are summarized in the form of Fig. 5, though a detailed calculation procedure will be described subsequently.

Let us first discuss the case where $0 < e/a < 0.5$. In this case, a rotational failure such as shown in Fig. 4 is possible to occur in the solid below the circular footing. The failure arc in the meridional plane ($x = 0$) has a length equal to the distance AE. The slip circle in the solid starts from point E, extends deepest in the solid below point B and meets the surface of the solid again at a point that is opposite to point E, with respect to the dotted line indicated.

The failure arc in a vertical plane with $a \geq x \neq 0$ will meet the periphery of the footing with a shorter radius of slip. If we denote such a radius of slip by $g(x)$, then

$$\begin{aligned} g_1(x) &= \sqrt{(c + \sqrt{a^2 - x^2})^2 + (z_0)^2} \\ g_2(x) &= \sqrt{(c - \sqrt{a^2 - x^2})^2 + (z_0)^2}. \end{aligned} \tag{3}$$

Here subscript 1 refers to the situation where a circular slip starts from somewhere on arc DEF, whereas subscript 2 refers to the situation where a shallower circular slip starts somewhere on arc DC or FG.

Let $\dot{W}_{int}$ be the rate of internal dissipation over an element $dA = g_i(x)d\theta\sqrt{(dx)^2 + (dg_i(x))^2}$, where $i = 1$ or 2. Let ω be the angular velocity of rotation about the x-axis.

$$d\dot{W}_{int} = k \cdot g_i(x)\omega dA = k \cdot g_i(x)\omega \cdot g_i(x)d\theta\sqrt{1 + \left(\frac{dg_i(x)}{dx}\right)^2}\,dx \tag{4}$$

Note here that the slip mode is symmetrical with respect to the meridional plane ($x = 0$).

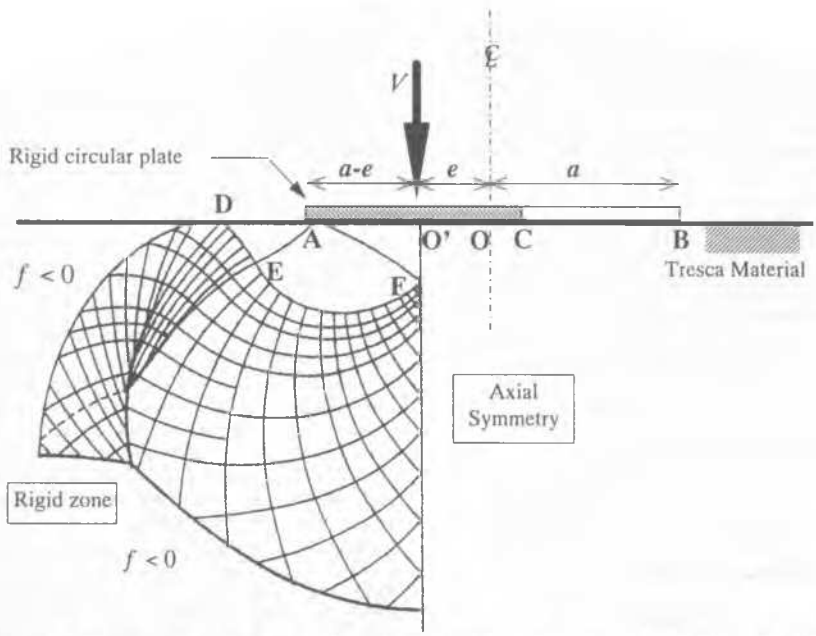

Figure 3: Construction of a statically admissible stress field below a circular rigid footing

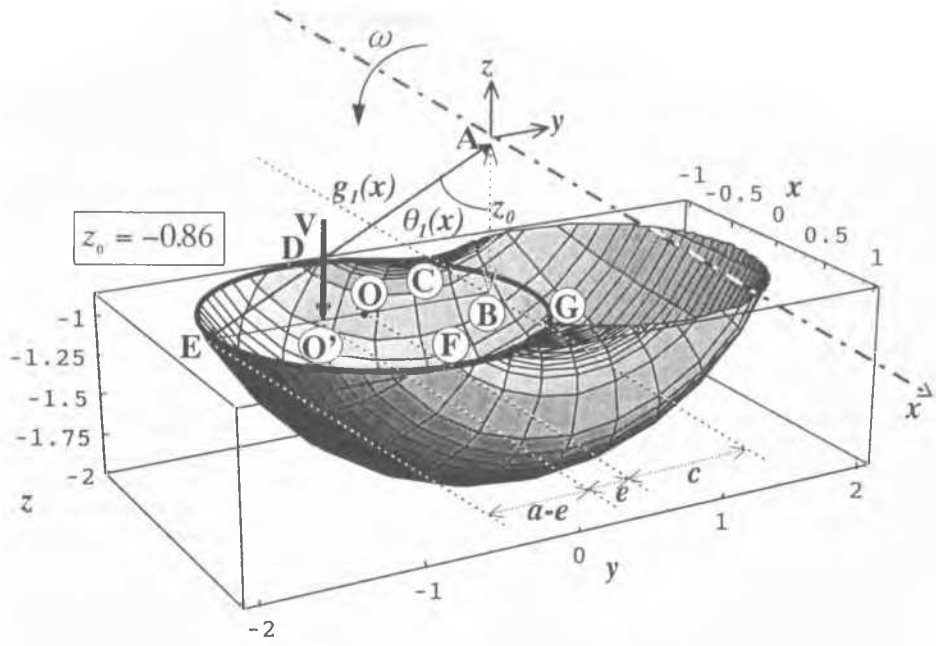

Figure 4: Circular rigid footing undergoing rotational failure mechanism

Then, integration of the rate of internal dissipation over a total slip area permits the total dissipation rate $\dot{W}_{int}$ to be expressed as

$$\dot{W}_{int} = 4k\omega \int_0^a \{g_1\}^2 \theta_1 \sqrt{1+\left(\frac{dg_1}{dx}\right)^2}\,dx + 4k\omega \int_\eta^a \{g_2\}^2 \theta_2 \sqrt{1+\left(\frac{dg_2}{dx}\right)^2}\,dx \qquad (5)$$

where $\eta = \sqrt{a^2-c^2}$.

The angles $\theta_1(x)$ and $\theta_2(x)$ that appear in Eq. (5) are defined by

$$\theta_1(x) = \tan^{-1}\frac{c+\sqrt{a^2-x^2}}{z_o}, \quad \theta_2(x) = \tan^{-1}\frac{c-\sqrt{a^2-x^2}}{z_o}. \qquad (6)$$

The rate of external work done by the eccentric vertical load V may be expressed as

$$\dot{W}_{ext} = V \cdot a\omega\left(\frac{e}{a}+\frac{c}{a}\right). \qquad (7)$$

Equating $\dot{W}_{int}$ with $\dot{W}_{ext}$ leads the average pressure V/A to be given by

$$\frac{V}{A} = \frac{4k}{\pi}\frac{1}{e+c}\left\{\int_0^a (g_1)^2\theta_1\sqrt{1+\left(\frac{g_1}{dx}\right)^2}\,dx + \int_\eta^a (g_2)^2\theta_2\sqrt{1+\left(\frac{dg_2}{dx}\right)^2}\,dx\right\}. \qquad (8)$$

The above equation indicates that for a given eccentricity e, the average vertical pressure, V/A, over a given circular footing is a function of two geometrical parameters c and z_0.

Accordingly, the best upper-bound solution for a given eccentricity should be obtained by minimizing the expression on the right-hand side of Eq. (8), with respect to c and z_0. It was found in this regard that such minimization procedure may be simplified by setting

$$c/a = 1 - 2(e/a). \qquad (9)$$

Note that this assumption is kinematically compatible, and that point B is now located opposite to point E with respect to the loading point O' (Fig. 4).

A range of upper-bound calculations for $0 < e/a < 0.5$ were numerically performed by following the procedure described above. These results are plotted in Fig. 5 with solid rectangles.

Let us next discuss the case where the eccentricity e is in the range : $0.5 \leq e/a \leq 1.0$. In this case, integration in Eq. (8) for the g_1 term should be performed over a modified interval $[0, \eta]$. The contribution from the g_2 term does not occur due to the deformation mode assumed, and therefore it can simply be neglected.

A range of upper-bound calculations were numerically performed and are plotted in Fig. 5 with solid circles. It is seen that these plots coupled with the solid rectangles aforementioned appear to form a continuous curve, which approximates to a parabola.

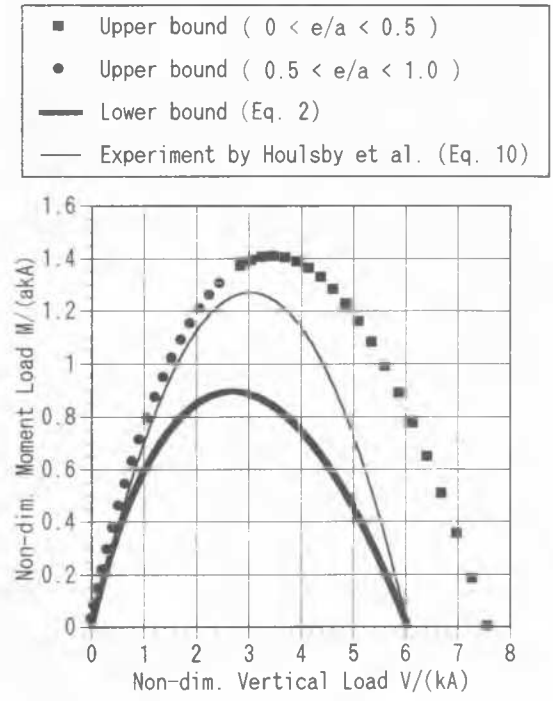

Figure 5: Lower- and upper-bound solutions for circular footings subjected to eccentric vertical loading

3 DISCUSSION

A comparison of the upper- and lower-bound solutions in Fig. 5 will indicate that these bearing capacity curves are similar in shape and are reasonably close to each other. The lower bound solution shows that the normalized maximum vertical capacity is equal to $V/(kA) = 6.05$, which is the exact solution for centered vertical loading. The peak moment capacity is found to be equal to $M_{pk}/(akA) = 0.90$ when $V/(kA) = 2.69$. The upper bound solution shows that the maximum vertical capacity is $V_m/(kA) = 7.61$ and that the peak moment capacity becomes equal to $M_{pk}/(akA) = 1.41$ when $V/(kA) = 3.51$.

To check the validity of these limit analyses, we discuss experimental results from circular spud-can footing tests (Houlsby & Martin, 1993). It is of interest to mention that a spud-can footing has received considerable practical interest, since it may serve as an economic and movable platform foundation for offshore hydro-carbon extraction structures. The 'average' experimental results of bearing capacity of circular spud-can footings on clay foundations obtained by Houlsby & Martin (1993) are expressed as

$$\frac{M}{M_{pk}} = 4\frac{V}{V_m}\left(1 - \frac{V}{V_m}\right), \tag{10a}$$

$$M_{pk} \approx 0.21 V_m \cdot a \tag{10b}$$

where V_m and M_{pk} are the limit vertical capacity under centered vertical loading and the maximum moment capacity under eccentric vertical loading, respectively.

It is important to note that the average experimental curve shown in Fig. 5 using Eq. (10) falls nicely in the band which is bracketed by the proposed plastic solutions.

4 CONCLUSIONS

This paper has discussed the bearing capacity of a circular rigid footing subjected to eccentric vertical loading resting on a weightless Tresca material. The results obtained may be summarized as follows.

- The effective circular area shown in Fig. 2 was used to find a statically admissible stress field. The consequent form of bearing capacity (Eq. (2)) was a lower-bound plastic solution compatible with lower-bound theorem. The shape of this solution on the plane $V/(kA)$ versus $M/(akA)$ was shown in Fig. 5.
- A three-dimensional collapse mechanism, shown in Fig. 4, was proposed to evaluate the upper bound solution (Fig. 5).
- The exact solution is bounded by the upper- and the lower-bound solutions shown in Fig. 5. The shapes of the upper- and lower-bound were similar to each other and corresponded well to the average experimental results of Houlsby & Martin (1993) using spud-can footings on clay.

  This suggests potential practical applications for the approach described in this paper.

REFERENCES

Butterfield, R. & G. Gottardi 1994. A complete three-dimensional failure envelope of shallow footings on sand. *Géotechnique* 44(1): 181–184.

Dean, E. T. R., R. G. James, A. N. Schofield, F. S. C. Tan & Y. Tsukamoto 1993. The bearing capacity of conical footings on sand in relation to the behavior of spudcan footing of jackups. *Predictive Soil Mechanics*: 165–178. London: Thomas Telford.

Eason, G. & R. T. Shield 1960. The plastic indentation of a semi-infinite solid by a perfectly rough circular punch. *Journal of Applied Mathematics and Physics (ZAMP)* 11: 33–43.

Hansen, J. B. 1961. General formula for bearing capacity. *Bulletin of The Danish Technical Institute* 11: 38–46.

Houlsby, G. T. & C. M. Martin 1993. Modelling of the behaviour of foundations of jack-up units on clay. *Predictive Soil Mechanics* : 339–358. London: Thomas Telford.

Meyerhof, G. G. 1953. The bearing capacity of foundations under eccentric and inclined loads. *Proc. 3rd ICSMFE* : 440–445.

Nova, R. & L. Montrasio 1991. Settlements of shallow foundations on sand. *Géotechnique* 41(2): 243–256.